20 Sep 2017

Potency and Cytotoxicity of a Novel Gallium-Containing Mesoporous Bioactive Glass/Chitosan Composite Scaffold as Hemostatic Agents

Sara Pourshahrestani

Ehsan Zeimaran

Nahrizul Adib Kadri

Nicola Gargiulo

et. al. For a complete list of authors, see https://scholarsmine.mst.edu/che_bioeng_facwork/1099

Recommended Citation

S. Pourshahrestani et al., "Potency and Cytotoxicity of a Novel Gallium-Containing Mesoporous Bioactive Glass/Chitosan Composite Scaffold as Hemostatic Agents," *ACS Applied Materials and Interfaces*, vol. 9, no. 37, pp. 31381 - 31392, American Chemical Society, Sep 2017.
The definitive version is available at https://doi.org/10.1021/acsami.7b07769

ACS APPLIED MATERIALS & INTERFACES

Research Article

www.acsami.org

Potency and Cytotoxicity of a Novel Gallium-Containing Mesoporous Bioactive Glass/Chitosan Composite Scaffold as Hemostatic Agents

Sara Pourshahrestani,*[,†] Ehsan Zeimaran,[†,∥] Nahrizul Adib Kadri,*[,†] Nicola Gargiulo,[⊥] Hassan Mahmood Jindal,[‡] Sangeetha Vasudevaraj Naveen,[§] Shamala Devi Sekaran,[‡] Tunku Kamarul,[§] and Mark R. Towler*[,†,#]

[†]Department of Biomedical Engineering, Faculty of Engineering, [‡]Department of Medical Microbiology, Faculty of Medicine, and [§]Tissue Engineering Group (TEG), National Orthopaedic Centre of Excellence in Research and Learning (NOCERAL), Department of Orthopaedic Surgery, Faculty of Medicine, University of Malaya, 50603 Kuala Lumpur, Malaysia

[∥]School of Engineering, Monash University, 47500 Bandar Sunway, Selangor, Malaysia

[⊥]ACLabs - Laboratori di Chimica Applicata, Dipartimento di Ingegneria Chimica, dei Materiali e della Produzione Industriale, Università Federico II, P.le Tecchio 80, 80125 Napoli, Italy

[#]Department of Mechanical & Industrial Engineering, Ryerson University, Toronto M5B 2K3, Ontario, Canada

ABSTRACT: Chitosan-based hemostats are promising candidates for immediate hemorrhage control. However, they have some disadvantages and require further improvement to achieve the desired hemostatic efficiency. Here, a series of 1% Ga_2O_3-containing mesoporous bioactive glass−chitosan composite scaffolds (Ga-MBG/CHT) were constructed by the lyophilization process and the effect of various concentrations of Ga-MBG (10, 30, and 50 wt %) on the hemostatic function of the CHT scaffold was assessed as compared to that of Celox Rapid gauze (CXR), a current commercially available chitosan-coated hemostatic gauze. The prepared scaffolds exhibited >79% porosity and showed increased water uptake compared to that in CXR. The results of coagulation studies showed that pure CHT and composite scaffolds exhibited increased hemostatic performance with respect to CXR. Furthermore, the composite scaffold with the highest Ga-MBG content (50 wt %) had increased capability to enhancing thrombus generation, blood clotting, and platelet adhesion and aggregation than that of the scaffold made of pure CHT. The antibacterial efficacy and biocompatibility of the prepared scaffolds were also assessed by a time-killing assay and an Alamar Blue assay, respectively. Our results show that the antibacterial effect of 50% Ga-MBG/CHT was more pronounced than that of CHT and CXR. The cell viability results also demonstrated that Ga-MBG/CHT composite scaffolds had good biocompatibility, which facilitates the spreading and proliferation of human dermal fibroblast cells even with 50 wt % Ga-MBG loading. These results suggest that Ga-MBG/CHT scaffolds could be a promising hemostatic candidate for improving hemostasis in critical situations.

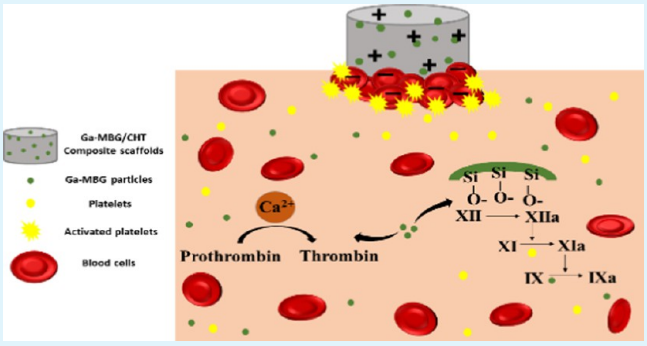

KEYWORDS: *mesoporous bioactive glass, gallium, chitosan, hemostatic property, hemostasis*

1. INTRODUCTION

Globally, severe trauma leading to uncontrolled hemorrhage is a global public health problem. Traumatic injury accounts for about 1 out of 10 mortalities, causing more than 5.8 million deaths worldwide annually,[1,2] which is predicted to rise to over 8 million by 2020.[1,3]

Bacterial infections at the wound sites are another major concern for the wound repair, which can impair the natural healing process because of abscess formation, even leading to life-threatening sepsis.[4,5] Hence, immediate control of hemorrhage by applying hemostatic agents and dressings with efficient antibacterial property can increase the survival rate and reduce bleeding complications and pathogen contamination. Although some encouraging results have been achieved, there are complications associated with the commercial hemostats that cannot be neglected. For instance, dry fibrin sealant dressings, although enhancing blood coagulation via the provision of a high local concentration of coagulation factors, are known to transmit viral infections;[6] collagen-based hemostatic agents produce allergic reactions[7] and can cause nerve compression and damage due to excessive swelling;[8] and cellulose is less effective against profuse bleeding and irregular lacerations. The acidic nature of cellulose products is known to cause not only inflammation of surrounding tissue but also delay in wound healing.[9] Hemostats based on inorganic species, including zeolites (i.e., QuikClot and QuikClot Advanced Clotting

Received: June 1, 2017
Accepted: August 24, 2017
Published: August 24, 2017

DOI: 10.1021/acsami.7b07769
ACS Appl. Mater. Interfaces 2017, 9, 31381−31392

Sponge Plus), can lead to thermal tissue injuries by the resulting exothermic reaction and elicit a foreign-body response owing to their poor biodegradability. They have also proven to be ineffective in controlling arterial bleeding.[8,10,11] Clay-based hemostatic agents (i.e., QuickClot Combat Gauze and WoundStat), which belong to another group of inorganic hemostats, are often unable to achieve rapid hemostasis, resulting in more extensive blood loss than that from other hemostats.[11,12] Furthermore, these materials have been found to be less effective in coagulopathic patients and can induce toxicity, embolization, and tissue inflammation.[11]

More recently, chitosan-based hemostatic agents (i.e., HemCon, TraumaStat, and Celox) have demonstrated superior efficiency relative to other hemostats in inducing hemostasis and improving survival.[13] Chitosan, a positively charged polysaccharide, is an N-deacetylated chitin derivative[14] and found in the exoskeleton of crustaceans.[15] It has a great significance for the development of hemostatic biomaterials due to possessing desirable features, such as biodegradability,[16] biocompatibility, nontoxicity,[17] antimicrobial and anti-inflammatory activity,[18] and inherent hemostatic properties.[19,20]

However, chitosan-based hemostats face several drawbacks that may limit their application. As an example, HemCon, while offering potent hemostasis in animal hemorrhage models and in some clinical trials, was later abandoned because of the lack of efficacy in controlling excessive bleeding;[12,21−23] moreover, Celox induced a strong inflammatory response at the surrounding tissues despite possessing many of the ancillary characteristics of an ideal hemostatic dressing.[12]

Additionally, these hemostats exhibited variable hemostatic performance when tested in animal models of extremity arterial hemorrhage.[24] For instance, although the dressings were able to stop low-pressure arterial bleeding, they failed to maintain hemostasis once fluid resuscitation was administered to return the blood pressure to the baseline range. Indeed, recovering blood pressure led to rebleeding that started as adherence of the dressings failed.[24] These results suggest that chitosan lacks sufficient capability to forming a mechanically stable hemostatic plug. To overcome these problems, a number of strategies have been proposed to enhance the antihemorrhagic effect of chitosan-based hemostats.[15,25−27] One of the most promising solutions to achieve this goal is the modification of the physicochemical properties of chitosan by incorporation of inorganic fillers into its matrix and fabrication of a composite scaffold with impressive blood-clotting abilities.[28−30] Ong et al.[29] prepared a series of silver-loaded chitosan−polyphosphate composites and found that the incorporation of polyphosphate polymers into the chitosan matrix can increase the blood clotting rate and lead to more potent hemostasis. In addition, Liu et al.[30] observed that the hemostatic activity of chitosan scaffolds can be improved by incorporating a clay mineral, halloysite nanotubes (HNTs), into their structure. The authors observed that increasing the HNT content into the chitosan matrix not only improved the mechanical properties (Young's modulus, compressive strength, and toughness) of the chitosan scaffold but also increased the blood-clotting abilities of the scaffold compared to those of pure chitosan.[30] Although these chitosan-based scaffolds were found to possess efficient hemostatic properties, nondegradability of the filler[30] and cytotoxic effects of the materials toward fibroblast cells, resulting from silver release from the dressing,[29,31] may raise safety concerns over these materials and limit their application for hemorrhage control. The obvious way to greatly improve the hemostatic efficacy of chitosan, while maintaining its biodegradability and biocompatibility, is therefore to design a chitosan-based composite material, using a biodegradable and nontoxic hemostatic inorganic filler.

In the past few years, mesoporous bioactive glasses (MBGs), a new class of nanostructured materials, have shown promise for hemostatic clinical application due to their unique features, such as highly ordered mesoporous channel structure, high porosity, and huge surface area and pore volume.[32−36]

In our previous study, we found that tuning the composition of a MBG with incorporation of low concentration of therapeutic gallium ions (Ga^{3+}) into its matrix not only enhanced its capability of platelet aggregation, thrombus formation, and blood coagulation activation but also improved its biodegradability and biocompatibility.[37]

In the present study, we endeavored to assess the possibility of using 1% Ga-MBG/chitosan composite scaffolds (Ga-MBG/CHT) to produce rapid hemostatic effects. In this regard, the Ga-MBG/CHT composite scaffolds with three different 1% Ga-MBG contents (10, 30, and 50 mol %) were prepared by a lyophilization method. The influence of 1% Ga-MBG on the microstructure, physicochemical properties, in vitro hemostatic efficacy, antibacterial efficacy, and cytocompatibility of CHT scaffolds was investigated. The hemostatic activity of the Ga-MBG/CHT composite scaffolds was also compared to that of a commercially available Celox Rapid gauze (CXR; Medtrade Products, Crewe, U.K.).

2. EXPERIMENTAL SECTION

2.1. Synthesis of Ga-MBG Powders. Ga-MBG powders (1%; molar ratio: Si/Ca/P/Ga = 79:15:5:1) were prepared by an evaporation-induced self-assembly (EISA) process following a procedure described elsewhere.[37] Briefly, gallium(III)nitrate hydrate ($Ga(NO_3)_3{\cdot}xH_2O$), tetraethyl orthosilicate (TEOS), calcium nitrate tetrahydrate ($Ca(NO_3)_2{\cdot}4H_2O$), and triethyl phosphate (TEP) were dissolved in ethyl alcohol (EtOH, Merck) containing 0.5 M nitric acid (HNO_3) and the resulting solution was stirred at room temperature overnight. To undergo the EISA process, the obtained sol was introduced in a Petri dish at room temperature for several days, followed by calcination at 600 °C for 5 h to remove the template. The obtained glass was ground and sieved to obtain particles below 32 μm. All of the precursors were purchased from Sigma-Aldrich and were of analytical grade (≥98%).

2.2. Preparation of Ga-MBG/CHT Composite Scaffolds. Porous Ga-MBG/CHT composite scaffolds with three different concentrations of 1% Ga-MBG (10, 30, and 50 wt %) were prepared using a freeze-drying technique. In detail, 1 g of CHT (Medium molecular weight, 85% deacetylated, Sigma-Aldrich) was dissolved in 1% acetic acid (v/v, 100 mL) and vigorously stirred overnight. Then, the calculated amounts of 1% Ga-MBG powders (10, 30, and 50 wt %) were added in the CHT solution. After continuously stirring overnight, the solution was then homogenized by means of an ultrasonic bath (ST-UB5200LT, SASTEC) for 30 min. Afterward, 0.1% (v/v) glutaraldehyde solution as the cross-linking agent was dropped in the Ga-MBG/CHT solution followed by stirring at room temperature for 1 h. Subsequently, 0.2 mL of each solution was immediately transferred into the wells of 96-well plates or 1 mL in 24-well plates. To obtain porous Ga-MBG/CHT composite scaffolds, the plates were then placed in a freezer at −20 °C overnight followed by lyophilization at −50 °C using a freeze-drying machine (FreeZone 2.5, LABCONCO, 7670531) for 24 h. To neutralize the residual acetic acid, the scaffolds were immersed in 2% NaOH for 2 h and then rinsed with distilled water several times. The scaffolds were finally frozen followed by freeze-drying at −50 °C and storage in a drying box at room temperature for further use. The obtained composites were named 10% Ga-MBG/CHT, 30% Ga-MBG/CHT, and 50% Ga-

DOI: 10.1021/acsami.7b07769
ACS Appl. Mater. Interfaces 2017, 9, 31381−31392

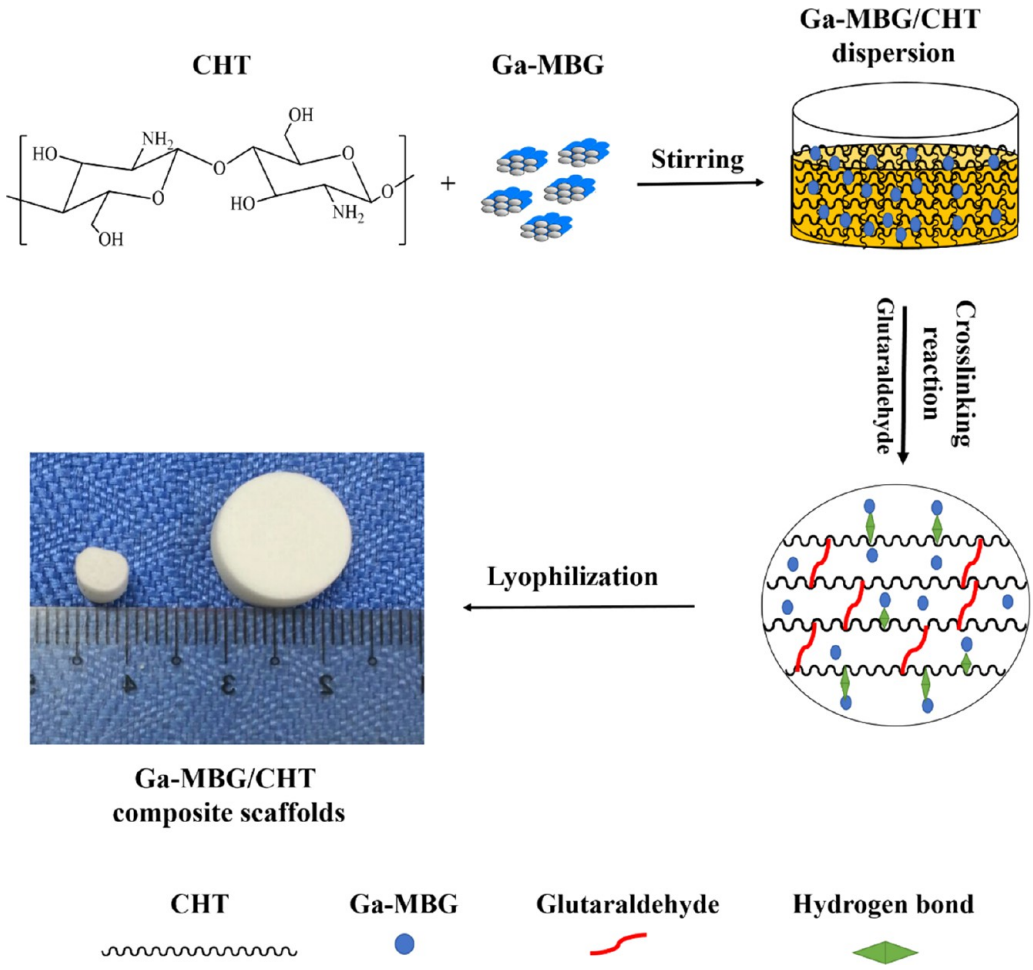

Figure 1. Schematic representation demonstrating the fabrication process of the Ga-MBG/CHT composite scaffolds. The hydrogen bond between CHT and Ga-MBG may be formed by interaction of NH_2 and OH groups of CHT with silanol groups of Ga-MBG. Another possibility is that CHT can react with cationic ions of Ga-MBG (i.e., Ca^{2+} and Ga^{3+}) through its functional groups.

MBG/CHT containing 10, 30, and 50 wt % Ga-MBG, respectively. Pure CHT scaffolds served as control and were fabricated in the same way but without addition of Ga-MBG. Figure 1 schematically depicts the steps of preparation of the composite scaffolds.

2.3. Physicochemical Characterization of Ga-MBG and Ga-MBG/CHT Composite Scaffolds. To investigate the pore structure of 1% Ga-MBG, small-angle XRD (SAXRD) patterns were recorded on a X-ray diffractometer (PANalytical Empyrean) using Cu Kα radiation (λ = 0.154 nm, 40 kV, 45 mA) in the 2θ range of 0.6–5°. High-resolution transmission electron microscopy (HRTEM) micrographs were obtained on a JEOL JEM-2100F microscope operated at 200 kV to assess the internal microstructure of the glass powders. The dispersion and distribution of the glass particles into the CHT matrix were also investigated by HRTEM. Prior to the observation, the scaffolds were embedded in epoxy resin (Ted Pella) and ultrathin sections of the samples with a thickness of approximately 80 nm were prepared using an ultramicrotome (RMC PowerTome PC) with a diamond knife (RMC diamond knife). N_2 adsorption–desorption isotherms at 77 K were obtained using Micromeritics Tristar II 3020 for determining the textural properties of the glass and scaffolds. To obtain surface area, the Brunauer–Emmett–Teller (BET) method was applied. The pore size distribution was also determined by the Barret–Joyner–Halenda method. The surface morphology and pore structure of pure CHT and the composite scaffolds were assessed by field emission scanning electron microscopy (FESEM: Quantat 250 FEG-FEI) at an accelerating voltage of 5 kV. Prior to FESEM observations, all of the samples were sputter-coated with gold. Wide-angle X-ray diffraction (WAXRD) data of the glass and scaffolds were collected using a PANalytical Empyrean diffractometer, operated at 40 kV and 40 mA with Cu Kα radiation (λ = 0.154 nm). The diffraction patterns were recorded in the 2θ range of 10–50° (step size: 0.02° and counting time: 5 s per step). Attenuated total reflectance Fourier Transform infrared (ATR-FTIR) spectroscopy (Spectrum 400, Perkin Elmer) was employed to characterize the composite scaffolds in the wavelength range of 400–4000 cm^{-1}.

2.4. Determination of Porosity. The porosity of the prepared composite scaffolds was measured by a liquid displacement method.[38] A certain volume (V_1) of ethanol was added into a graduated cylinder, the samples were then immersed into the cylinder until they were saturated by absorbing ethanol, and the reading was recorded as V_2. After the scaffolds were removed, the volume of the remaining solution (V_3) was recorded, followed by measuring the porosity (%) as $[(V_1 - V_3)/(V_2 - V_3)]$.

2.5. Phosphate Buffer Saline Absorption. The absorption efficiency of the scaffolds was determined in phosphate buffer saline (PBS, pH 7.4) solution. The preweighed dry scaffolds (W_{dry}) were suspended in 1 mL of PBS in a 24-well plate, followed by incubation for 2 h in an incubator at 37 °C. The scaffolds were then taken out and gently dabbed on an absorbent paper towel to remove the excess surface water, and the wet weight of the samples was then immediately measured (W_{wet}). Fluid uptake of the scaffolds (%) was calculated as $(W_{wet} - W_{dry})/W_{dry}$.

2.6. In Vitro Thrombus Formation on Ga-MBG/CHT Composite Scaffolds. The induced thrombotic effects of the Ga-MBG/CHT composite scaffolds compared to those of CXR were evaluated according to the literature.[37,39] Citrated human blood (9:1 whole blood to 3.2% sodium citrate) was freshly collected from healthy volunteers (University of Malaya Human Ethical Committee -

DOI: 10.1021/acsami.7b07769
ACS Appl. Mater. Interfaces 2017, 9, 31381–31392

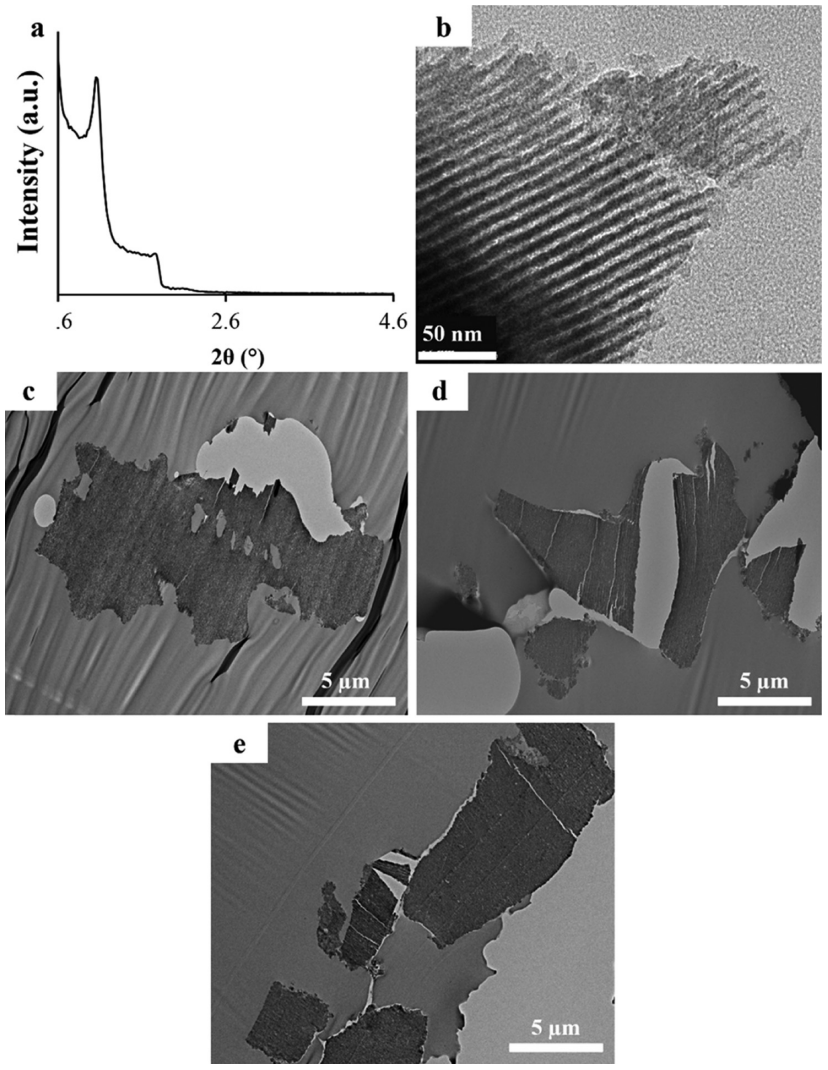

Figure 2. (a) SAXRD of 1% Ga-MBG. TEM images of (b) Ga-MBG, (c) 10% Ga-MBG/CHT, (d) 30% Ga-MBG/CHT, and (e) 50% Ga-MBG/CHT. The images of the scaffolds captured after epoxy resin embedding and microtome sectioning. Ga-MBG and CHT appear in dark gray and white, respectively.

approval 967.10, UMMC). The thrombus formation was initiated by adding 1 mL of citrated blood to the preweighed scaffolds (W_o), which have been already placed in 24-well plates at 37 °C. After 30 min of incubation, 10 mL of deionized water was carefully dropped into well plates without blood clot disruption. After fixing the thrombus formed by 37% formaldehyde solution for 10 min, samples were dried in oven at 50 °C and their weights were recorded as W_t. The thrombogenicity of the scaffolds was calculated on the basis of the following equation

$$\text{Thrombogenicity (\%)} = [(W_t - W_o)/W_o] \times 100\%$$

2.7. Whole Blood Clotting Tests. To measure the blood-clotting ability of the Ga-MBG/CHT scaffolds, a blood clotting test adopted from Shih et al. was used.[40] Briefly, 0.1 mL of citrated human blood was slowly dropped to the scaffolds in polypropylene tubes and coagulation was triggered by adding 10 μL of $CaCl_2$ (0.2 M) solution. After incubation of the scaffolds for 10 min with shaking (30 rpm) at 37 °C, unstable blood clots were dissolved by adding 12.5 mL of distilled water. A microplate reader (BMG LABTECH, Offenburg, Germany) was used to determine the absorbance of hemoglobin solution at 544 nm.

2.8. In Vitro Platelet Adhesion. A lactate dehydrogenase (LDH) assay was utilized to quantify platelet adhesion levels on the Ga-MBG/CHT scaffolds by measuring the LDH released from the lysed platelets according to the reported literature.[25,37] Acid citrate dextrose-anticoagulated human blood was collected from healthy donors, and platelet-rich plasma (PRP) was obtained as previously described.[37] The samples were soaked in the platelet suspension and incubated at 37 °C for 30 min. To lyse the adhered platelets, the samples were then dip-rinsed thrice in PBS and incubated with 1% Triton X-100 in PBS at 37 °C for 1 h. The number of adhered platelets on the surfaces of the scaffolds and CXR was quantified using a LDH assay kit (Sigma-Aldrich). The morphology of the adhered platelets was also visualized by FESEM after the platelets were fixed in 2.5% glutaraldehyde followed by dehydration and drying in a graded series of ethanol and hexamethyldisilazane, respectively.

2.9. Antimicrobial Efficacy. To evaluate the antibacterial activity of the Ga-MBG/CHT scaffolds, the time-killing assay was used as described previously with minor modifications.[41] Briefly, two bacteria, *Escherichia coli* (E. coli) and *Staphylococcus aureus* (S. aureus), were grown overnight on Muller Hinton Agar (MHA). Few bacterial colonies were transferred into 1.5 mL Eppendorf tubes containing 1 mL of Luria-Bertani (LB) broth and spectrophotometrically adjusted to give an OD_{625} of 0.08−0.1, which is equivalent to $1-2 \times 10^8$ CFU/mL. The bacterial suspensions were serially diluted to give a final number of 1×10^6 CFU/mL. Each bacterial suspension (0.3 mL) was then transferred into 15 mL tubes containing the scaffolds and 2.7 mL of LB broth to give a final volume of 3 mL with bacterial number of 1×10^5 CFU/mL. All of the samples were incubated in a shaking incubator at 37 °C. At four different time points (0, 3, 6, and 24 h), 10

DOI: 10.1021/acsami.7b07769
ACS Appl. Mater. Interfaces 2017, 9, 31381−31392

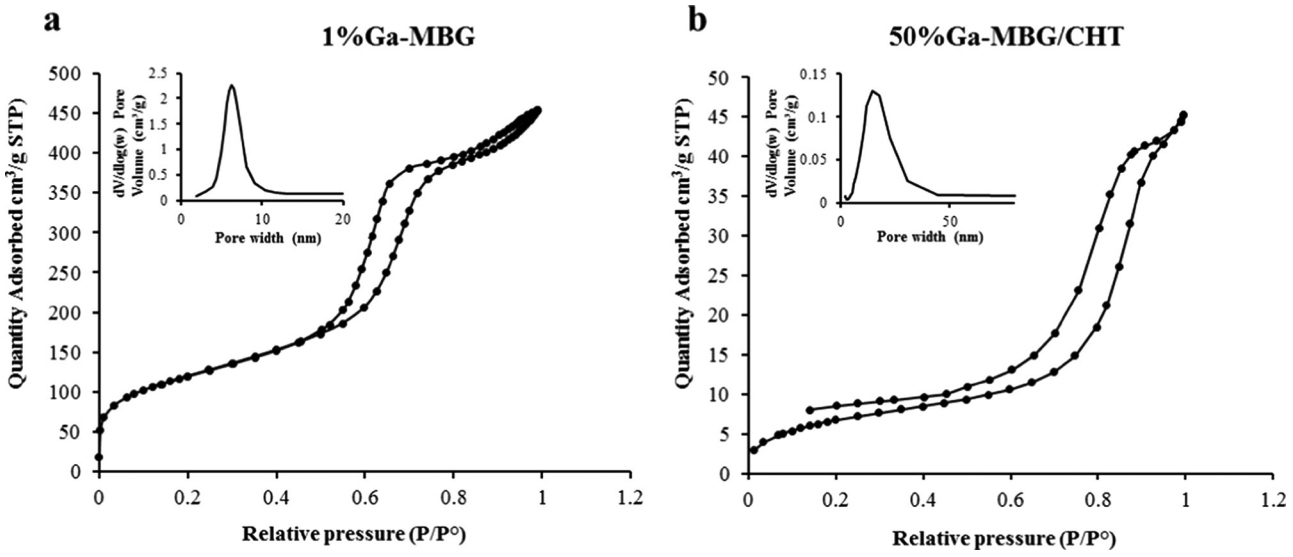

Figure 3. N_2 adsorption−desorption isotherms of (a) 1% Ga-MBG and (b) 50% Ga-MBG/CHT. Insets of both graphs depict the corresponding pore size distributions.

μL of each sample was serially diluted and plated on MHA for cell counting.

2.10. In Vitro Cytotoxic Evaluation. Proliferating and live cells were analyzed by the Alamar Blue assay. Alamar Blue quantifies the cells indirectly based on the cellular metabolism. Briefly, live proliferating cells reduce the blue color resazurin (an active ingredient of AB reagent) to a red color resorufin. Prior to performing the assay, the composite scaffolds were sterilized with 70% ethanol for 3 h, washed thrice with PBS, and soaked in L-Dulbecco's modified Eagle's medium until the cells were added. Dermal fibroblast cells obtained from humans (HDFs) were seeded on the materials (1×10^6 cells per well) in a 24-well plate (Ultra Low attachment plate), allowed to attach on the scaffolds and grow for 2 days, and then serum-starved for 24 h to arrest the cell cycle. Then, the experimental analysis was continued for day 1, 4, and 8 in triplicate, and scaffolds without cells served as negative controls. Eight hours before the stipulated time, 10% (v/v) of Alamar Blue was added directly in the experimental plate and incubated. The absorbance of the incubated media was measured at 570 and 600 nm.

2.11. Confocal Laser Scanning Microscopy. To further verify the cell viability results, fluorescence imaging was also employed as explained previously.[42] A live/dead solution was prepared by dissolving 5 μL of 4 mM calcein AM (Biotium) and 20 μL of 2 mM EthD-III (Biotium) in 10 mL of PBS. The scaffolds and CXR were then dark-incubated with the solution for 30 min. Images were obtained with a fluorescence microscope (Leica TCS SP5 II, Leica Microsystems, Mannheim, Germany) at excitation/emission wavelengths of 495/515 nm.

2.12. Statistical Analysis. Data collected in the present study was represented as the mean ± standard deviations, and statistical data analyses were carried out using SPSS software (version 22). To assess differences between two independent groups, the nonparametric Mann−Whitney *U*-test was employed. *P* values less than 0.05 were considered statically significant.

3. RESULTS

3.1. Physicochemical Characterization of Ga-MBG and Ga-MBG/CHT Composite Scaffolds. Figure 2a,b indicates the SAXRD pattern and HRTEM image of 1% Ga-MBG powders, respectively. From the SAXRD pattern (Figure 2a), two distinct diffraction peaks at around 2θ = 1.07 and 1.79° revealed that 1% Ga-MBG powders have highly ordered two-dimensional hexagonal (Plane Group *P6mm*) mesostructures. This result was further confirmed by TEM, which demonstrated that the 1% Ga-MBG powders consist of well-defined mesoporous channels. To explore whether the glass with different concentrations was distributed throughout the CHT and maintained its mesoporous structure after incorporation into the CHT matrix, the scaffolds were also examined by TEM. Figure 2c−e displays representative TEM images of the composite scaffolds. All of the micrographs demonstrated dispersion of 1% Ga-MBG in the CHT matrix. The images also illustrated the ordered mesoporous arrays of Ga-MBG embedded in the CHT scaffold matrix.

N_2 adsorption/desorption isotherms of 1% Ga-MBG and CHT with the highest glass content (50% Ga-MBG/CHT) together with their corresponding pore size distributions (inset graphs) are shown in Figure 3. Table 1 presents the main textural parameters of 1% Ga-MBG and all of the scaffolds as measured by N_2 adsorption porosimetry. As indicated in Figure 3a, 1% Ga-MBG revealed a type-IV isotherm with a hysteresis loop of type H1, as peculiar of materials with a mesoporous structure and cylindrical pores. The specific surface area and average pore size of 1% Ga-MBG were 435 $m^2\ g^{-1}$ and 6 nm, respectively. N_2 adsorption/desorption analysis also showed a type-IV isotherm pattern for Ga-MBG/CHT scaffolds, indicating the presence of mesopores in the scaffolds. However, the samples exhibited low-pressure hysteresis in their N_2 adsorption/desorption isotherm. The isotherm of the 50% Ga-MBG/CHT composite scaffold is depicted in Figure 3b. As expected, incorporating 1% Ga-MBG into CHT scaffolds influenced the textural properties of the CHT scaffolds. With increasing the glass content, the surface areas of the composite

Table 1. Pore Structure Parameters of 1% Ga-MBG, CHT, and Composite Scaffolds

samples	S_{BET} ($m^2\ g^{-1}$)	pore volume ($cm^3\ g^{-1}$)	average pore diameter (nm)
1% Ga-MBG	435	0.61	6.02
CHT	8.49	0.002	21.15
10% Ga-MBG/CHT	8	0.005	13.06
30% Ga-MBG/CHT	22	0.04	10.52
50% Ga-MBG/CHT	25	0.06	11.39

DOI: 10.1021/acsami.7b07769
ACS Appl. Mater. Interfaces 2017, 9, 31381−31392

scaffolds were increased, and 30% Ga-MBG/CHT and 50% Ga-MBG/CHT were found to have much higher surface areas (22 and 25 m^2 g^{-1}, respectively) than those of pure CHT scaffolds (8.49 m^2 g^{-1}) (Table 1). The pore volume of the composites also increased when more 1% Ga-MBG was incorporated into the CHT matrix. However, the average pore diameter of the scaffolds decreased with the increasing glass content.

The surface morphologies of the composite scaffolds and CXR were examined by FESEM. The micrographs of the composite scaffolds showed that all of the scaffolds possess interconnected porous structures and, in the case of the Ga-MBG/CHT samples, with an increase in the Ga-MBG content, more Ga-MBG particles were observed on the surface and interior of the scaffolds. The inner morphology and microstructure of pure CHT, 50% Ga-MBG/CHT, and CXR are depicted in Figure 4. The pure CHT sample exhibited a smooth

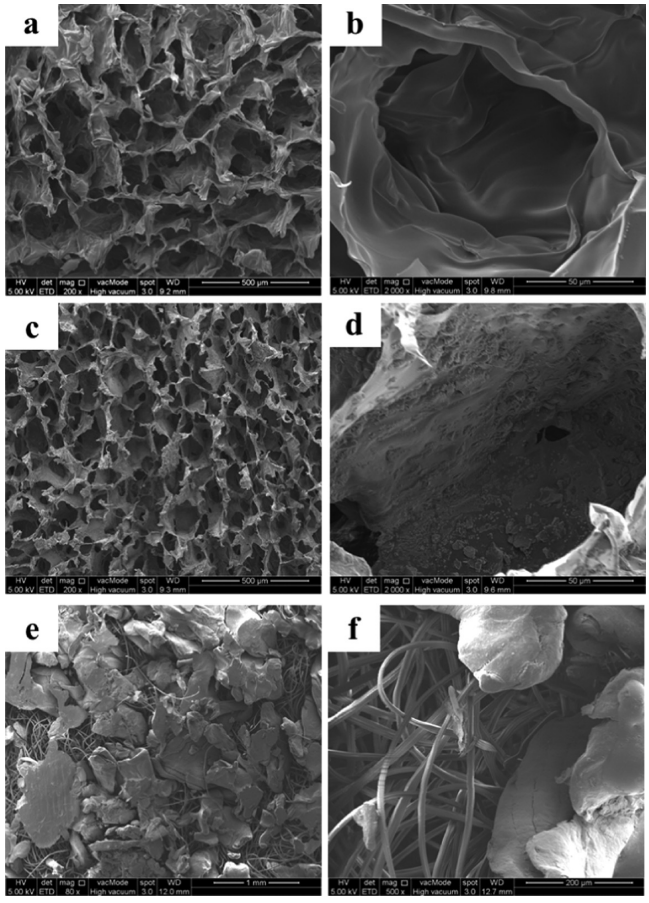

Figure 4. Surface morphologies of the samples under low and high magnifications. FESEM images of (a, b) pure CHT, (c, d) 50% Ga-MBG/CHT, and (e, f) CXR.

surface, and no particle was found on its surface (Figure 4a,b), whereas in 50% Ga-MBG/CHT, many Ga-MBG particles were deposited on the pore walls and/or embedded in the polymer phase (Figure 4c,d). FESEM imaging of CXR also showed that the gauze comprised fibers and chitosan flakes (Figure 4e,f).

The microstructures of Ga-MBG/CHT scaffolds were further investigated by WAXRD. Figure 5a compares WAXRD patterns of 1% Ga-MBG, CHT, and Ga-MBG/CHT scaffolds. A wide diffraction peak between 20 and 30° was observed for 1% Ga-MBG powders, which is characteristic of amorphous materials. The CHT scaffold exhibited a broad peak at around 2θ = 20.09°, indicating its semicrystalline nature. Figure 5a also indicates that the Ga-MBG/CHT scaffolds possess the characteristic peaks for both CHT and amorphous 1% Ga-MBG.

The chemical structure of Ga-MBG/CHT composite scaffolds was evaluated by FTIR and compared to that of 1% Ga-MBG and CHT. As represented in Figure 5b, the characteristic absorption peaks of CHT corresponding to the saccharide structure were identified at around 895 and 1151 cm^{-1} due to C−O−C vibrations of the glycosidic linkage. The peak at 1369 cm^{-1} is assigned to the C−H/N−H vibration.[43] Other characteristic absorption peaks of CHT appeared at about 1646 and 1566 cm^{-1}, that can be attributed to amide I C═O stretching and amide II N−H bending modes, respectively.[43] The FTIR spectra of 1% Ga-MBG also showed absorption bands at 1067 and 798 cm^{-1}, which are ascribed to the Si−O−Si asymmetric and symmetric stretching vibrations, respectively.[44] Figure 5b also presents the FTIR spectra of the composite scaffolds depicting the characteristic bands correlated to both CHT and 1% Ga-MBG.

3.2. Porosity. The total porosity of pure CHT and Ga-MBG/CHT composite scaffolds is listed in Table 2.

The results suggested that varying the 1% Ga-MBG content in the CHT matrix from 10 to 50 wt % can affect the total porosity of the composite scaffolds so that a trend toward decreased porosity was observed with the increasing Ga-MBG content. Although the pure CHT scaffold had the highest porosity with a value of 91.4%, the porosity diminished to 79.2% for 50% Ga-MBG/CHT.

3.3. PBS Absorption Efficiency in Vitro. A comparison of the PBS absorption efficiencies of pure CHT and Ga-MBG/CHT composite scaffolds with CXR is given in Figure 6. The results showed that, after 2 h of immersion in PBS, CHT (1572.3%), 10% Ga-MBG/CHT (1446.3%), 30% Ga-MBG/CHT (1116.2%), and 50% Ga-MBG/CHT (900.7%) scaffolds absorbed significantly more PBS solution with respect to their initial weight compared with CXR (585.9%). However, the PBS absorbability of the composite scaffolds decreased with the increasing amount of 1% Ga-MBG, which may be related to a decrease in their porosity.

3.4. Thrombus Formation. The thrombogenicity effect of the Ga-MBG/CHT composite scaffolds was examined and compared to that of pure CHT and CXR. The results depicted in Figure 7 indicated that much more thrombus was formed on the surface of the scaffolds with respect to CXR. The comparison between the scaffolds also revealed that the thrombogenicity ratio increased as the glass content increased in the polymer matrix, whereas 50% Ga-MBG/CHT resulted in higher thrombus formation on its surface with respect to pure CHT.

3.5. Whole Blood Clotting. The hemostatic potential of Ga-MBG/CHT composite scaffolds with respect to CXR was investigated by determining the absorbance of hemoglobin in uncoagulated blood (Figure 8a). As an indicative of blood clotting activity, the samples with a lower value of hemoglobin absorbance have demonstrated a higher capability to trapping red blood cells (RBCs) and forming clots. Although CXR had the greatest average absorbance value, indicating its lower coagulation efficiency, whole blood on CHT scaffolds demonstrated progressively greater clotting with the increasing 1% Ga-MBG content. As can be seen from Figure 8a, CHT with 50 wt % glass content led to a significantly lower absorbance value than that of the other tested samples. The

DOI: 10.1021/acsami.7b07769
ACS Appl. Mater. Interfaces 2017, 9, 31381−31392

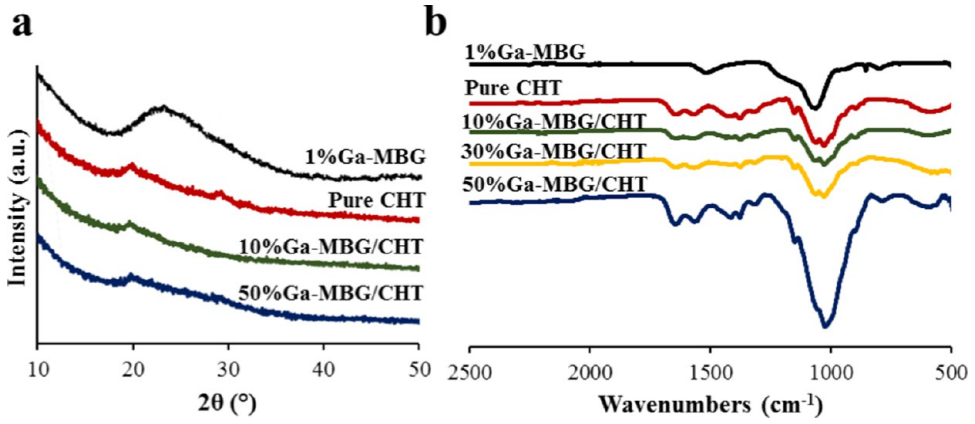

Figure 5. (a) WAXRD patterns of 1% Ga-MBG, pure CHT, 10% Ga-MBG/CHT, and 50% Ga-MBG/CHT composite scaffolds. (b) FTIR spectra of 1% Ga-MBG, pure CHT, and composite scaffolds.

Table 2. Porosity of the Composite Scaffolds

sample name	porosity
pure CHT	91.4% ± 8.6
10% Ga-MBG/CHT	88.6% ± 3.7
30% Ga-MBG/CHT	84.3% ± 5.4
50% Ga-MBG/CHT	79.2% ± 3.3

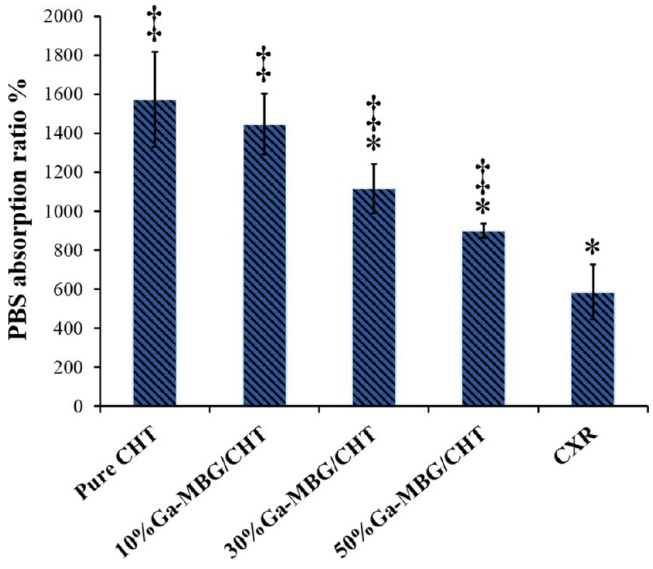

Figure 6. PBS absorption ratio of pure CHT, 10% Ga-MBG/CHT, 30% Ga-MBG/CHT, 50% Ga-MBG/CHT, and CXR. * and ‡ represent a significant difference with respect to CHT and CXR at $p < 0.05$, respectively.

whole blood interaction with the scaffolds and CXR was also photographed by a digital camera. Less blood was leached out of 50% Ga-MBG/CHT as compared to that from other scaffolds and CXR, confirming the aforementioned results. Furthermore, this result was consistent with that of thrombus formation tests.

3.6. Platelet Adhesion. Platelets, as a key component of blood, mainly contribute to preventing and/or ceasing bleeding via formation of a platelet plug. In this study, the ability of Ga-MBG/CHT composite scaffolds to stimulate platelet adhesion and aggregation was investigated in comparison to that of CHT and CXR after the materials were contacted with PRP suspensions for 30 min. Whereas the fewest numbers of

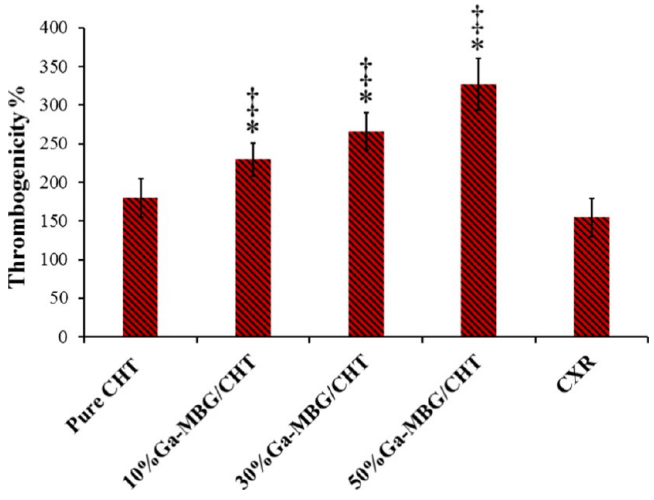

Figure 7. Effect of samples on thrombus formation over 30 min of incubation with whole blood. * and ‡ demonstrate a significant difference compared with CHT and CXR at $p < 0.05$, respectively.

adherent platelets were found on the CXR surface, more platelets adhered onto the CHT scaffolds with a higher amount of the glass (30% Ga-MBG/CHT and 50% Ga-MBG/CHT), representing their remarkable potential to evoke platelet adhesion and activation (Figure 9a). These results were further confirmed by FESEM, where the surface of 50% Ga-MBG/CHT (Figure 9d,e) demonstrated a large number of adhered platelets with lots of "pseudopods" stretching out with respect to CHT (Figure 9b,c) and CXR (Figure 9f,g).

3.7. Antibacterial Activity. The antibacterial feature of the CHT scaffolds was assessed against the Gram positive (*S. aureus*) and negative (*E. coli*) bacteria as compared to that of CXR. Figure 10 illustrates the antibacterial activities of the tested samples by the time-killing assay. Although none of the pure CHT and composite scaffolds were able to completely kill the bacteria after 24 h of treatment, the number of *E. coli* and *S. aureus* cells treated with the samples were less as compared to those treated with the negative control (LB broth culture). Additionally, 30% Ga-MBG/CHT and 50% Ga-MBG/CHT found to have a better antibacterial effect against both pathogens than that of pure CHT and CXR, resulting in lower bacterial viability.

3.8. In Vitro Cytotoxicity Evaluation. Figure 11 illustrates the effects of the scaffolds on the viability of HDF cells in

DOI: 10.1021/acsami.7b07769
ACS Appl. Mater. Interfaces 2017, 9, 31381−31392

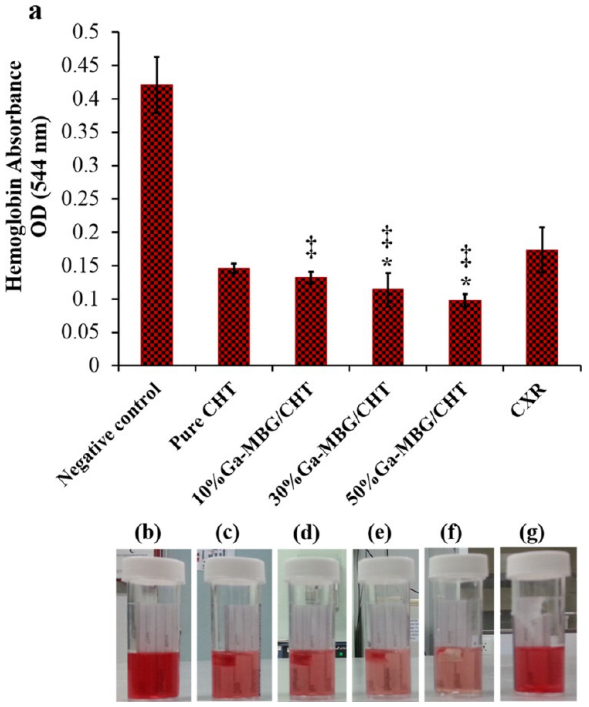

Figure 8. (a) Blood clotting rate of scaffolds and CXR as determined by measuring hemoglobin absorbance. (b–g) Photographs depicting more hemoglobin leaked from pure CHT, 10% Ga-MBG/CHT, and CXR than that from 30% Ga-MBG/CHT and 50% Ga-MBG/CHT. * and ‡ represent a significant difference with respect to CHT and CXR at $p < 0.05$, respectively.

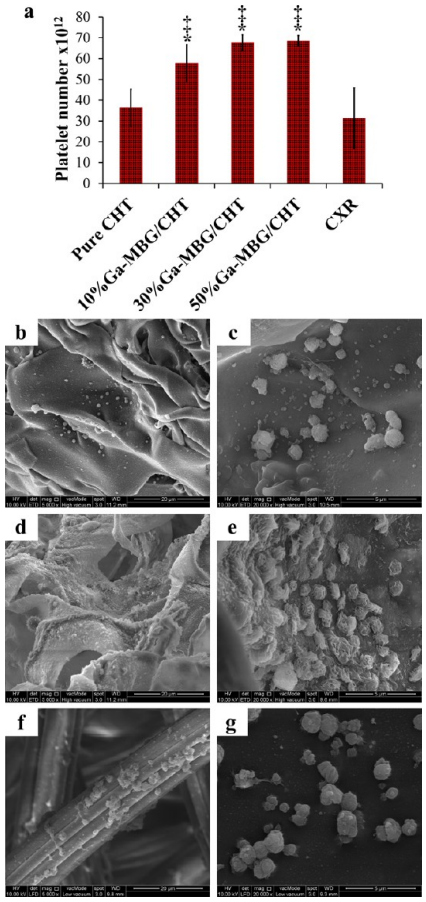

Figure 9. (a) Effect of materials on platelet adhesion after 30 min of incubation with PRP. Low- and high-magnification FESEM images of platelets adhered to the surfaces of (b, c) pure CHT, (d, e) 50% Ga-MBG/CHT, and (f, g) CXR. * and ‡ represent a significant difference in comparison to CHT and CXR at $p < 0.05$, respectively.

comparison to those of CXR. It has been shown that the cell count is linearly proportional to the amount of reduction of resazurin in Alamar Blue to resorufin. As illustrated in Figure 11a, the Alamar Blue reduction values for all of the samples increased with increasing the culture time, demonstrating their noncytotoxity toward HDF cells. Whereas CXR demonstrated a higher Alamar Blue reduction value with respect to the scaffolds at days 1 and 4, there was no statistical difference between the scaffolds during the incubation periods (Figure 11a). However, an obvious trend of increment in the Alamar Blue reduction values was observed for 30% Ga-MBG/CHT, 50% Ga-MBG/CHT, and CXR in comparison to that of pure CHT and 10% Ga-MBG/CHT after 8 days of culture. To further confirm the biocompatibility of the samples, cell viability was examined by a live/dead assay. The representative fluorescence images (Figure 11b) revealed that all of the materials were cytocompatible toward HFD cells as a large number of viable cells were observed on the surface of the materials after 4 days of culture.

4. DISCUSSION

Hemostasis is the multifaceted response of the body to hemorrhage and is divided into primary and secondary procedures. During primary hemostasis, a robust primary hemostatic plug is formed, which is strengthened to form a stable and permanent plug through secondary hemostasis (coagulation cascade).[45,46] Hence, hemostats should exert their hemostatic function to help in the formation of reinforced plug.

Chitosan-based hemostatic agents are the most current generation of hemostatic dressings that were found to be superior to other hemostats for improving the survival rate in animal models and treating prehospital combat casualties.[13] However, such dressings showed variable performances in injury models of high-pressure arterial bleeding and further research is therefore required to improve their efficacy to stop bleeding. Recently, we have proposed and developed 1% Ga_2O_3-substituted MBGs for use to staunch bleeding.[37] In the following work, we extend our previous study and fabricated a series of hemostatic composite scaffolds composed of chitosan and various concentrations of 1% Ga-MBG (10, 30, and 50 wt %) through a freeze-drying method and tested their ability to inducing rapid hemostasis in vitro. We believe that incorporating 1% Ga-MBG as an inorganic phase into the CHT matrix could combine the outstanding properties of both materials to enhance the hemostatic performance of the composite scaffolds.

Large amounts of RBCs can aggregate and immobilize onto CHT by electrostatic interaction between its positively charged surface and negatively charged neuraminic acid present on the surface of RBCs.[47] This interaction neutralizes the negative charges on the surface of RBCs and causes their irreversible deformation, which thus accelerates the clot formation. On the other hand, 1% Ga-MBG, as described previously, can activate the intrinsic coagulation pathway, which in turn accelerates thrombin generation and subsequent fibrin formation.[37] The results of this study proved that increasing the glass content from 10 to 50 wt % in the CHT matrix not only affected the physicochemical properties of CHT scaffolds but also played a

DOI: 10.1021/acsami.7b07769
ACS Appl. Mater. Interfaces 2017, 9, 31381–31392

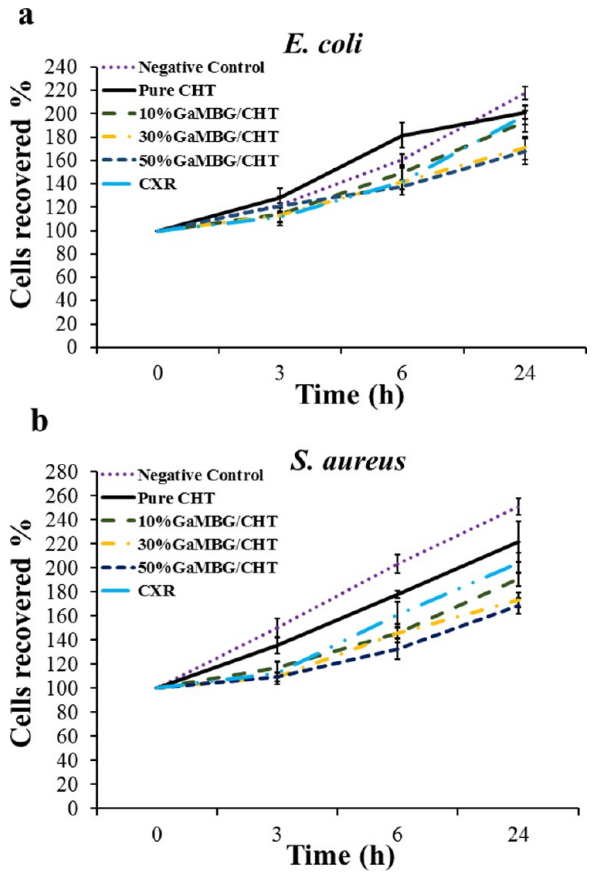

Figure 10. In vitro time-killing assay of samples against (a) *E. coli* and (b) *S. aureus*.

crucial role in enhancing the hemostatic events as CHT with the highest glass content (50 wt %) could obviously promote blood clotting with respect to other samples.

High water absorption capacity of a hemostatic agent could benefit to absorb water from blood flow in the wounded area, concentrating blood components, such as platelets and RBCs, and enhancing the blood coagulation. The results from water uptake measurements indicated that the presence of Ga-MBG modified water absorption in the composite scaffolds (Figure 6). The percentage of hydration decreased with the increase of Ga-MBG concentration. One of the possible explanations for this phenomenon can be associated with the porosity of the composite scaffolds that slightly decreased with the incorporation of Ga-MBG into the CHT matrix. Such a decrease could also be explained by the interaction of the OH and NH_2 groups of CHT with the silanol groups of Ga-MBG and therefore by the unavailability of such groups for hydrogen bonding with water molecules. Additionally, the decrease in water absorption can be attributed to an increase in the cross-linking density of the Ga-MBG/CHT scaffolds resulting from the increase in the Ga-MBG content.

These results are in accordance with those presented by Maji et al.[48] According to these authors, increasing the 58S bioglass content in chitosan−gelatin scaffolds can lead to a decreased water absorption.[48] However, the water absorption capacity of the composite scaffolds was still good enough for hemostatic application as they revealed higher hemostatic ability compared to that of pure CHT and CXR. These results evidenced that other parameters can also contribute to the hemostatic efficacy of the composite scaffolds.

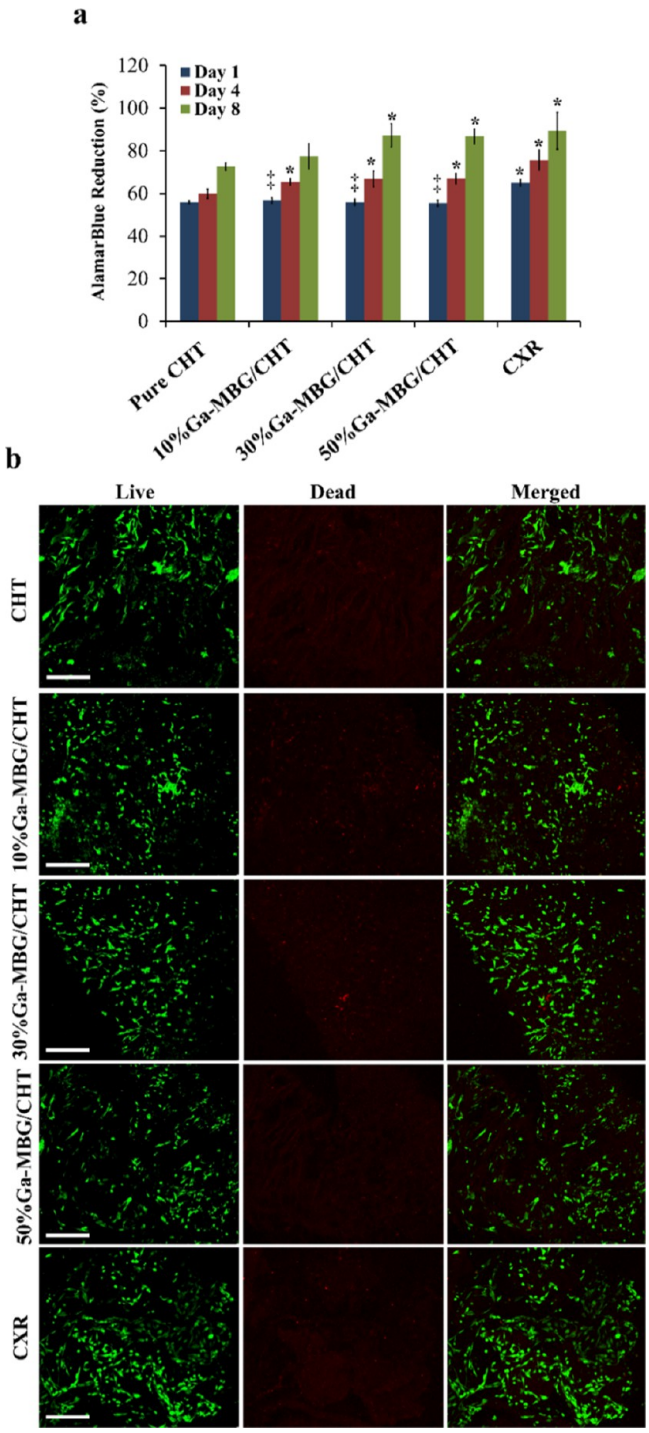

Figure 11. (a) Cytotoxic effects of CHT, Ga-MBG/CHT composite scaffolds, and CXR on HDF cells. (b) Fluorescence micrographs of live (green), dead (red), and merged images of HDF cells treated with CHT, 10% Ga-MBG/CHT, 30% Ga-MBG/CHT, 50% Ga-MBG/CHT, and CXR after 4 days of culture. * and ‡ represent a significant difference in comparison to CHT and CXR at $p < 0.05$, respectively.

The results of the thrombus formation assay (Figure 7) clearly disclose that the incorporation of 1% Ga-MBG into the CHT matrix can affect the thrombogenicity of the CHT scaffold. Interestingly, the Ga-MBG/CHT composite scaffolds, particularly 50% Ga-MBG/CHT, resulted in higher thrombus formation compared to that from CHT and CXR. A possible explanation is as follows: in addition to chitosan that exerts its

DOI: 10.1021/acsami.7b07769
ACS Appl. Mater. Interfaces 2017, 9, 31381−31392

hemostatic effect through its positively charged, protonated amino groups (NH_3^+) and interacts strongly with negatively charged RBCs, the glass content also contributes to the thrombogenic potential of the composite scaffolds. At higher glass contents, the Ga-MBG/CHT composite scaffolds may have a higher ability to releasing Ca^{2+} ions from the glass framework into the blood. As previously explained, Ca^{2+} ions not only contribute to the activation of the intrinsic pathway but also help to produce thrombin, a serine protease that is reported to be involved in fibrin clot generation.[32,37] Thus, the thrombin production and subsequent fibrin formation could increase the thrombus RBC content on Ga-MBG/CHTs. These results were consistent with the result of the whole blood clotting assay (Figure 8), where the CHT scaffolds with a higher amount of Ga-MBG exhibited a lower absorbance value, suggesting their higher clotting performance.

In the platelet adhesion analysis, both composite scaffolds containing 30 and 50 wt % glass enhanced the platelet adhesion compared with pure CHT and CXR and there was no significant difference between them (Figure 9a). FESEM micrographs (Figure 9b–g) also demonstrated more activated platelets with protruding pseudopods on the 50% Ga-MBG/CHT surface than those of pure CHT and CXR.

These results suggest that 30% Ga-MBG/CHT and 50% Ga-MBG/CHT may have higher Ca^{2+} ion release rates compared to those of 10% Ga-MBG/CHT. This favorable factor can significantly contribute to the production of the proteolytic enzyme thrombin and lead to faster platelet adhesion and activation.[49] The high ability of the scaffolds to enhance platelet adhesion and aggregation can also be ascribed to the ability of chitosan to absorb fibrinogen and various circulating plasma proteins, which are adsorbed onto the material surface, thereby promoting platelet adhesion.[29]

The results of the time-killing assay (Figure 10) demonstrated that the incorporation of a higher amount of glass into CHT matrix improved its antibacterial property against both examined pathogens as compared with that of CHT, CXR, and pure LB broth culture. The higher antibacterial activity of 30% Ga-MBG/CHT and 50% Ga-MBG/CHT is thought to be related to the combined characteristics of CHT and Ga-MBG. On one hand, it is believed that CHT exerts its antimicrobial activity through destabilizing and disrupting cell membranes,[50] resulting from the electrostatic interactions between its NH_3^+ groups and the phosphoryl groups of phospholipid, a main components of cell membranes, containing negative charge.[51] On the other hand, Ga-MBG, as previously confirmed,[37] was found to have antibacterial activity due to the presence of Ga^{3+} and the ability of changing pH when it is eluted from the scaffolds. Therefore, as expected, the antibacterial property of pure CHT was enhanced with the addition of Ga-MBG into its matrix.

The cytocompatibility of the Ga-MBG/CHT composite scaffolds in comparison to that of CHT and CXR was evaluated according to the metabolic activity of HDF cells using the Alamar Blue assay. The results showed that HDF cell viability and proliferation on the composites and CXR were increased (Figure 11a). It is noted that cell response to the biomaterials is affected by both the chemical composition and the degree of surface roughness.[52] Distribution of Ga-MBG in the CHT matrix not only changed the chemical composition of the scaffolds but also increased the surface roughness of the scaffolds. It has been previously highlighted that the bioactive glasses can release the ions (i.e., Si^{4+} and Ca^{2+}) into fluid that stimulate biocompatibility.[53,54] Therefore, Ga-MBG with high ionic leaching ability and enhancing the surface roughness of the scaffolds may stimulate HDF cell responses, leading to good cytocompatibility.

Overall, the above results indicate that the prepared Ga-MBG/CHT composite scaffolds have a greater potential for use as hemostatic agents in comparison to CHT and CXR. On the basis of the results of the hemostatic assays, 50% Ga-MBG/CHT was found to be superior to other samples in promoting hemostasis as it resulted in higher thrombus formation, faster clotting rate, and increased platelet adhesion and aggregation.

5. CONCLUSIONS

Ga-MBG/CHT composite scaffolds with different Ga-MBG contents were prepared by a lyophilization technique. Our results indicated that although incorporation of Ga-MBG led to slightly decreased water uptake and porosity of the CHT scaffolds it was in favor of enhancing the hemostatic performance, as the sample with the highest Ga-MBG content exhibited a higher blood clotting and platelet activation abilities compared with those of pure CHT and CXR. Our experimental results support the hypothesis that the synergistic effect of both CHT and Ga-MBG endow the composite scaffolds with high hemostatic efficacy. 30% Ga-MBG/CHT and 50% Ga-MBG/CHT illustrated better antimicrobial activity against *E. coli* and *S. aureus* bacteria in comparison to that of CHT and CXR. The cytotoxicity evaluations further highlighted the biocompatibility of the samples when in contact with HDF cells for 1, 4, and 8 days. This is the first demonstration of the potential usefulness of Ga-MBG/CHT composite scaffolds in accelerating hemostasis. The results demonstrated that our novel hemostatic composite scaffolds have great potential for clinical hemostatic applications. However, for clinical use, an understanding of their hemostatic activity in vivo is imperative.

AUTHOR INFORMATION

Corresponding Authors

*E-mail: sara.pourshahrestani@gmail.com. Tel: +60142023115 (S.P.).

*E-mail: nahrizuladib@um.edu.my. Tel: +603-79674581 (N.A.K.).

*E-mail: mtowler@Ryerson.ca. Tel: +1-416-979-5000 (ext. 4518) (M.R.T.).

ORCID

Nahrizul Adib Kadri: 0000-0001-9694-4337

Notes

The authors declare no competing financial interest.

ACKNOWLEDGMENTS

This research is supported by HIR-MoE Grant (Reference number-UM.C/625/1/HIR/ MOHE/CHAN/03, account number - A000003-50001), the University of Malaya Research Grants scheme (UMRG, RP038A-15HTM) and Postgraduate Research Grant (PPP: PG077-2015B).

REFERENCES

(1) Rossaint, R.; Bouillon, B.; Cerny, V.; Coats, T. J.; Duranteau, J.; Fernández-Mondéjar, E.; Filipescu, D.; Hunt, B. J.; Komadina, R.; Nardi, G.; et al. The European Guideline on Management of Major Bleeding and Coagulopathy Following Trauma. *Crit. Care* **2016**, *20*, 100.

DOI: 10.1021/acsami.7b07769
ACS Appl. Mater. Interfaces 2017, 9, 31381–31392

(2) Naghavi, M.; Wang, H.; Lozano, R.; Davis, A.; Liang, X.; Zhou, M. Gbd 2013 Mortality and Causes of Death Collaborators. Global, Regional, and National Age-Sex Specific All-Cause and Cause-Specific Mortality for 240 Causes of Death, 1990-2013: A Systematic Analysis for the Global Burden of Disease Study 2013. *Lancet* **2015**, *385*, 117−171.
(3) Murray, C. J.; Lopez, A. D. Alternative Projections of Mortality and Disability by Cause 1990−2020: Global Burden of Disease Study. *Lancet* **1997**, *349*, 1498−1504.
(4) Owens, C. D.; Stoessel, K. Surgical Site Infections: Epidemiology, Microbiology and Prevention. *J. Hosp. Infect.* **2008**, *70*, 3−10.
(5) Reichman, D. E.; Greenberg, J. A. Reducing Surgical Site Infections: A Review. *Rev. Obstet. Gynecol.* **2009**, *2*, 212−221.
(6) Pusateri, A. E.; Holcomb, J. B.; Kheirabadi, B. S.; Alam, H. B.; Wade, C. E.; Ryan, K. L. Making Sense of the Preclinical Literature on Advanced Hemostatic Products. *J. Trauma Acute Care Surg.* **2006**, *60*, 674−682.
(7) Seyednejad, H.; Imani, M.; Jamieson, T.; Seifalian, A. Topical Haemostatic Agents. *Br. J. Surg.* **2008**, *95*, 1197−1225.
(8) Achneck, H. E.; Sileshi, B.; Jamiolkowski, R. M.; Albala, D. M.; Shapiro, M. L.; Lawson, J. H. A Comprehensive Review of Topical Hemostatic Agents: Efficacy and Recommendations for Use. *Ann. Surg.* **2010**, *251*, 217−228.
(9) Tomizawa, Y. Clinical Benefits and Risk Analysis of Topical Hemostats: A Review. *J. Artif. Organs* **2005**, *8*, 137−142.
(10) Granville-Chapman, J.; Jacobs, N.; Midwinter, M. Pre-Hospital Haemostatic Dressings: A Systematic Review. *Injury* **2011**, *42*, 447−459.
(11) Pourshahrestani, S.; Zeimaran, E.; Djordjevic, I.; Kadri, N. A.; Towler, M. R. Inorganic Hemostats: The State-of-the-Art and Recent Advances. *Mater. Sci. Eng. C* **2016**, *58*, 1255−1268.
(12) Kheirabadi, B. Evaluation of Topical Hemostatic Agents for Combat Wound Treatment. *U.S. Army Med. Dep. J.* **2011**, *2*, 25−37.
(13) Bennett, B. L.; Littlejohn, L. F.; Kheirabadi, B. S.; Butler, F. K.; Kotwal, R. S.; Dubick, M. A.; Bailey, J. A. Management of External Hemorrhage in Tactical Combat Casualty Care: Chitosan-Based Hemostatic Gauze Dressings - Tccc Guidelines Change 13-05. *J. Spec. Oper. Med.* **2014**, *14*, 40−57.
(14) Rao, S. B.; Sharma, C. P. Use of Chitosan as a Biomaterial: Studies on Its Safety and Hemostatic Potential. *J. Biomed. Mater. Res.* **1997**, *34*, 21−28.
(15) Kang, P.-L.; Chang, S. J.; Manousakas, I.; Lee, C. W.; Yao, C.-H.; Lin, F.-H.; Kuo, S. M. Development and Assessment of Hemostasis Chitosan Dressings. *Carbohydr. Polym.* **2011**, *85*, 565−570.
(16) Yang, X.; Chen, X.; Wang, H. Acceleration of Osteogenic Differentiation of Preosteoblastic Cells by Chitosan Containing Nanofibrous Scaffolds. *Biomacromolecules* **2009**, *10*, 2772−2778.
(17) Bhattarai, N.; Edmondson, D.; Veiseh, O.; Matsen, F. A.; Zhang, M. Electrospun Chitosan-Based Nanofibers and Their Cellular Compatibility. *Biomaterials* **2005**, *26*, 6176−6184.
(18) Deng, H.; Lin, P.; Xin, S.; Huang, R.; Li, W.; Du, Y.; Zhou, X.; Yang, J. Quaternized Chitosan-Layered Silicate Intercalated Composites Based Nanofibrous Mats and Their Antibacterial Activity. *Carbohydr. Polym.* **2012**, *89*, 307−313.
(19) Chou, T.-C.; Fu, E.; Wu, C.-J.; Yeh, J.-H. Chitosan Enhances Platelet Adhesion and Aggregation. *Biochem. Biophys. Res. Commun.* **2003**, *302*, 480−483.
(20) Muzzarelli, R. A.; Morganti, P.; Morganti, G.; Palombo, P.; Palombo, M.; Biagini, G.; Belmonte, M. M.; Giantomassi, F.; Orlandi, F.; Muzzarelli, C. Chitin Nanofibrils/Chitosan Glycolate Composites as Wound Medicaments. *Carbohydr. Polym.* **2007**, *70*, 274−284.
(21) Cox, E. D.; Schreiber, M. A.; McManus, J.; Wade, C. E.; Holcomb, J. B. New Hemostatic Agents in the Combat Setting. *Transfusion* **2009**, *49*, 248S−255S.
(22) Rhee, P.; Brown, C.; Martin, M.; Salim, A.; Plurad, D.; Green, D.; Chambers, L.; Demetriades, D.; Velmahos, G.; Alam, H. Quikclot Use in Trauma for Hemorrhage Control: Case Series of 103 Documented Uses. *J. Trauma: Inj., Infect., Crit. Care* **2008**, *64*, 1093−1099.
(23) Acheson, E. M.; Kheirabadi, B. S.; Deguzman, R.; Dick, E. J., Jr.; Holcomb, J. B. Comparison of Hemorrhage Control Agents Applied to Lethal Extremity Arterial Hemorrhages in Swine. *J. Trauma: Inj., Infect., Crit. Care* **2005**, *59*, 865−875.
(24) Kheirabadi, B. S.; Scherer, M. R.; Estep, J. S.; Dubick, M. A.; Holcomb, J. B. Determination of Efficacy of New Hemostatic Dressings in a Model of Extremity Arterial Hemorrhage in Swine. *J. Trauma: Inj., Infect., Crit. Care* **2009**, *67*, 450−460.
(25) Lan, G.; Lu, B.; Wang, T.; Wang, L.; Chen, J.; Yu, K.; Liu, J.; Dai, F.; Wu, D. Chitosan/Gelatin Composite Sponge Is an Absorbable Surgical Hemostatic Agent. *Colloids Surf., B* **2015**, *136*, 1026−1034.
(26) Chan, L. W.; Kim, C. H.; Wang, X.; Pun, S. H.; White, N. J.; Kim, T. H. Polystat-Modified Chitosan Gauzes for Improved Hemostasis in External Hemorrhage. *Acta Biomater.* **2016**, *31*, 178−185.
(27) Feng, C.; Li, J.; Wu, G. S.; Mu, Y. Z.; Kong, M.; Jiang, C. Q.; Cheng, X. J.; Liu, Y.; Chen, X. G. Chitosan-Coated Diatom Silica as Hemostatic Agent for Hemorrhage Control. *ACS Appl. Mater. Interfaces* **2016**, *8*, 34234−34243.
(28) Liang, D.; Lu, Z.; Yang, H.; Gao, J.; Chen, R. Novel Asymmetric Wettable Agnps/Chitosan Wound Dressing: In Vitro and in Vivo Evaluation. *ACS Appl. Mater. Interfaces* **2016**, *8*, 3958−3968.
(29) Ong, S.-Y.; Wu, J.; Moochhala, S. M.; Tan, M.-H.; Lu, J. Development of a Chitosan-Based Wound Dressing with Improved Hemostatic and Antimicrobial Properties. *Biomaterials* **2008**, *29*, 4323−4332.
(30) Liu, M.; Shen, Y.; Ao, P.; Dai, L.; Liu, Z.; Zhou, C. The Improvement of Hemostatic and Wound Healing Property of Chitosan by Halloysite Nanotubes. *RSC Adv.* **2014**, *4*, 23540−23553.
(31) Fong, J.; Wood, F. Nanocrystalline Silver Dressings in Wound Management: A Review. *Int. J. Nanomed.* **2006**, *1*, 441−449.
(32) Dai, C.; Yuan, Y.; Liu, C.; Wei, J.; Hong, H.; Li, X.; Pan, X. Degradable, Antibacterial Silver Exchanged Mesoporous Silica Spheres for Hemorrhage Control. *Biomaterials* **2009**, *30*, 5364−5375.
(33) Ostomel, T. A.; Shi, Q.; Tsung, C. K.; Liang, H.; Stucky, G. D. Spherical Bioactive Glass with Enhanced Rates of Hydroxyapatite Deposition and Hemostatic Activity. *Small* **2006**, *2*, 1261−1265.
(34) Shruti, S.; Salinas, A. J.; Ferrari, E.; Malavasi, G.; Lusvardi, G.; Doadrio, A. L.; Menabue, L.; Vallet-Regi, M. Curcumin Release from Cerium, Gallium and Zinc Containing Mesoporous Bioactive Glasses. *Microporous Mesoporous Mater.* **2013**, *180*, 92−101.
(35) Salinas, A. J.; Shruti, S.; Malavasi, G.; Menabue, L.; Vallet-Regi, M. Substitutions of Cerium, Gallium and Zinc in Ordered Mesoporous Bioactive Glasses. *Acta Biomater.* **2011**, *7*, 3452−3458.
(36) Shruti, S.; Salinas, A. J.; Lusvardi, G.; Malavasi, G.; Menabue, L.; Vallet-Regi, M. Mesoporous Bioactive Scaffolds Prepared with Cerium-, Gallium-and Zinc-Containing Glasses. *Acta Biomater.* **2013**, *9*, 4836−4844.
(37) Pourshahrestani, S.; Zeimaran, E.; Kadri, N. A.; Gargiulo, N.; Samuel, S.; Naveen, S. V.; Kamarul, T.; Towler, M. R. Gallium-Containing Mesoporous Bioactive Glass with Potent Hemostatic Activity and Antibacterial Efficacy. *J. Mater. Chem. B* **2016**, *4*, 71−86.
(38) Yang, Y.; Zhao, J.; Zhao, Y.; Wen, L.; Yuan, X.; Fan, Y. Formation of Porous Plga Scaffolds by a Combining Method of Thermally Induced Phase Separation and Porogen Leaching. *J. Appl. Polym. Sci.* **2008**, *109*, 1232−1241.
(39) Imai, Y.; Nose, Y. A New Method for Evaluation of Antithrombogenicity of Materials. *J. Biomed. Mater. Res.* **1972**, *6*, 165−172.
(40) Shih, M.-F.; Shau, M.-D.; Chang, M.-Y.; Chiou, S.-K.; Chang, J.-K.; Cherng, J.-Y. Platelet Adsorption and Hemolytic Properties of Liquid Crystal/Composite Polymers. *Int. J. Pharm.* **2006**, *327*, 117−125.
(41) Jindal, H. M.; Le, C. F.; Yusof, M. Y. M.; Velayuthan, R. D.; Lee, V. S.; Zain, S. M.; Isa, D. M.; Sekaran, S. D. Antimicrobial Activity of Novel Synthetic Peptides Derived from Indolicidin and Ranalexin against *Streptococcus pneumoniae*. *PloS One* **2015**, *10*, No. e0128532.

DOI: 10.1021/acsami.7b07769
ACS Appl. Mater. Interfaces 2017, 9, 31381−31392

(42) Wang, M. O.; Etheridge, J. M.; Thompson, J. A.; Vorwald, C. E.; Dean, D.; Fisher, J. P. Evaluation of the in Vitro Cytotoxicity of Cross-Linked Biomaterials. *Biomacromolecules* **2013**, *14*, 1321−1329.
(43) Miola, M.; Verné, E.; Ciraldo, F. E.; Cordero-Arias, L.; Boccaccini, A. R. Electrophoretic Deposition of Chitosan/45s5 Bioactive Glass Composite Coatings Doped with Zn and Sr. *Front. Bioeng. Biotechnol.* **2015**, *3*, 159.
(44) Arcos, D.; Vila, M.; López-Noriega, A.; Rossignol, F.; Champion, E.; Oliveira, F.; Vallet-Regí, M. Mesoporous Bioactive Glasses: Mechanical Reinforcement by Means of a Biomimetic Process. *Acta Biomater.* **2011**, *7*, 2952−2959.
(45) Broos, K.; Feys, H. B.; De Meyer, S. F.; Vanhoorelbeke, K.; Deckmyn, H. Platelets at Work in Primary Hemostasis. *Blood Rev.* **2011**, *25*, 155−167.
(46) Behrens, A. M.; Sikorski, M. J.; Kofinas, P. Hemostatic Strategies for Traumatic and Surgical Bleeding. *J. Biomed. Mater. Res., Part A* **2014**, *102*, 4182−4194.
(47) Yang, J.; Tian, F.; Wang, Z.; Wang, Q.; Zeng, Y. J.; Chen, S. Q. Effect of Chitosan Molecular Weight and Deacetylation Degree on Hemostasis. *J. Biomed. Mater. Res., Part B* **2008**, *84*, 131−137.
(48) Maji, K.; Dasgupta, S.; Pramanik, K.; Bissoyi, A. Preparation and Evaluation of Gelatin-Chitosan-Nanobioglass 3d Porous Scaffold for Bone Tissue Engineering. *Int. J. Biomater.* **2016**, *2016*, No. 9825659.
(49) Coughlin, S. R. Thrombin Signalling and Protease-Activated Receptors. *Nature* **2000**, *407*, 258−264.
(50) Raafat, D.; von Bargen, K.; Haas, A.; Sahl, H.-G. Chitosan as an Antibacterial Compound: Insights into Its Mode of Action. *Appl. Environ. Microbiol.* **2008**, *74*, 3764−3773.
(51) No, H. K.; Park, N. Y.; Lee, S. H.; Meyers, S. P. Antibacterial Activity of Chitosans and Chitosan Oligomers with Different Molecular Weights. *Int. J. Food Microbiol.* **2002**, *74*, 65−72.
(52) Liu, M.; Wu, C.; Jiao, Y.; Xiong, S.; Zhou, C. Chitosan−Halloysite Nanotubes Nanocomposite Scaffolds for Tissue Engineering. *J. Mater. Chem. B* **2013**, *1*, 2078−2089.
(53) Zeimaran, E.; Mohan, S.; Pourshahrestani, S.; Pingguan-Murphy, B.; Kadri, N. A.; Murali, M. R.; Raghavendran, H. R. B.; Hasikin, K.; Kamarul, T.; Towler, M. R. Osteogenic Differentiation of Mesenchymal Stem Cells on a Poly (Octanediol Citrate)/Bioglass Composite Scaffold in Vitro. *Mater. Des.* **2016**, *109*, 434−442.
(54) Alcaide, M.; Portoles, P.; López-Noriega, A.; Arcos, D.; Vallet-Regí, M.; Portoles, M. Interaction of an Ordered Mesoporous Bioactive Glass with Osteoblasts, Fibroblasts and Lymphocytes, Demonstrating Its Biocompatibility as a Potential Bone Graft Material. *Acta Biomater.* **2010**, *6*, 892−899.

DOI: 10.1021/acsami.7b07769
ACS Appl. Mater. Interfaces 2017, 9, 31381−31392